Decay of Entropy From a Conservative Spectral Method for Fokker-Planck-Landau Type Equations

Clark A. Pennie[1,a)] and Irene M. Gamba[1,b)]

[1]*The University of Texas at Austin, Austin, TX 78712, USA*

[a)]Corresponding author: cpennie@math.utexas.edu
[b)]gamba@math.utexas.edu

Abstract. Expanding upon the conservative spectral method for solving the Landau equation, developed by Zhang and Gamba, a deterministic scheme has been developed for modeling Fokker-Planck-Landau type equations with Maxwell molecules and hard sphere interactions. The original case, corresponding to the classical physical problem of Coulomb interactions, is also included and the stability for all three scenarios investigated. The power of the method is exemplified through simulations demonstrating the decay of relative entropy for both Coulomb interactions and hard potentials. The Coulomb interaction example shows that there is a degenerate spectrum, with the relative entropy decaying at a rate close to the law of two thirds as predicted by Strain and Guo, while the hard potential example exhibits a spectral gap.

1 Introduction

An important model for plasmas is the Landau equation, which results from the grazing collision limit of the Boltzmann equation. This limit, first derived by Landau [1], assumes that colliding particles are travelling almost parallel to each other due to repulsive Coulomb forces. A more mathematical description of the limit was detailed by Villani [2] and Desvillettes and Villani [3], even for extended potential rates higher than Coulumb interactions and up to hard spheres. When rates different to Coulomb interactions are used, the equation is referred to as being of Fokker-Planck-Landau type. Computationally, the problem has been studied by Bobylev and Potapenko [4], using Monte Carlo methods, and in Fourier space by Haack and Gamba [5].

The Landau equation is rather difficult to model, either analytically or numerically, due to the high dimensionality, non-linearity and non-locality. For numerical simulations, a deterministic scheme can be used, such as the conservative spectral method, developed by Zhang and Gamba [6], which is the model of choice for the current work. Spectral methods were first considered as a model for the homogeneous Landau equation by Bobylev and Rjasanow [7] and Pareschi et al. [8]. The evolution of the Landau equation has also been simulated by means of a Monte-Carlo scheme for the Boltzmann equation with sufficiently singular angular cross-sections that cancel the Coulomb potential. This approach results in an expensive algorithm compared to the spectral-based methods.

The version of the spectral method in this work exploits the weak form of the Landau equation in order to calculate the Fourier transform of the collision operator. It does so in just $O(N^3 \log N)$ operations, where the number of Fourier modes N in each velocity dimension can be small, thanks to the conservation enforcement. For computational purposes, a cut-off domain in velocity space is used, within which the majority of the solution's mass should be supported, based on a result by Gamba et al. [9] for the Boltzmann equation. This general construction of a spectral method was first applied to the Boltzmann equation by Gamba and Tharkabhushaman [10] and the details for the derivation of the Landau equation scheme can be found in [6].

Pareschi's construction of a spectral method involved extending the solution periodically, which did not respect the decay of the solution toward infinity in velocity space. As a result, aliasing effects were noticed in their solution. Subsequently, Filbet and Pareschi [11] applied this idea to the inhomogeneous Landau equation by using a finite volume method in space but this scheme did not preserve the conservation properties of the Landau equation. A conservative method was later proposed by Crouseilles and Filbet [12], using centered finite differences, but this only conserved mass and energy, not momentum, and required certain symmetry properties of the initial data.

One particular attraction to the current method is its ability to yield the correct decay of entropy. The conservation enforcement is essential in the proof of convergence of the spectral method applied to the Boltzmann equation [13] and it is believed that the same should be true for Fokker-Planck-Landau type equations. The entropy decay rate is also a consequence of this fact. To the best of the authors' knowledge, this is the first time that the convergence rate of two thirds, proven analytically by Strain and Guo [14], has been seen through a numerical approximation of the relative entropy.

The method described in [6] is in fact a solver for the inhomogeneous Landau equation, coupled to Poisson's equation, where the advection is modeled by a discontinuous Galerkin scheme. Extensions of the relative entropy results in this work to the inhomogeneous case are in progress. In addition, this paper contains results for Fokker-Planck-Landau type equations associated to Maxwell molecules and hard spheres, expanding upon the previous work.

The layout of this work is as follows. First, the set up of the problem is described in section 2, along with any required definitions. The expressions for the Fourier transform of the Fokker-Planck-Landau type operators corresponding to Coulomb interactions, Maxwell molecules and hard spheres are derived in section 3 and the stability results given in section 4. Finally, section 5 contains the numerical results, demonstrating the correct decay rate to equilibrium for both Coulomb interactions and hard spheres. All work here is part of a PhD thesis by the first author, under advisorship of the second, and elaborated on in a future work by both authors [15].

2 Description of Problem

A space-homogeneous Fokker-Planck-Landau type equation for the probability density function (pdf) $f(t, \boldsymbol{v})$, where $(t, \boldsymbol{v}) \in (\mathbb{R}^+, \Omega_{\boldsymbol{v}})$, with $\Omega_{\boldsymbol{v}} \subseteq \mathbb{R}^3$, is of the form

$$f_t(t, \boldsymbol{v}) = \frac{1}{\varepsilon} Q(f, f)(t, \boldsymbol{v}), \tag{1}$$

where ε is the Knudsen number and $Q(f, f)$ is the collision operator given by

$$Q(f, f) = \nabla_{\boldsymbol{v}} \cdot \int_{\Omega_{\boldsymbol{v}}} S(\boldsymbol{v} - \boldsymbol{v}_*)(f_* \nabla_{\boldsymbol{v}} f - f \nabla_{\boldsymbol{v}_*} f_*) \, \mathrm{d}\boldsymbol{v}_*, \quad \text{for } S(\boldsymbol{u}) = |\boldsymbol{u}|^{\gamma+2} \left(\mathrm{I} - \frac{\boldsymbol{u}\boldsymbol{u}^T}{|\boldsymbol{u}|^2} \right),$$

with $-3 \leq \gamma \leq 1$, $I \in \mathbb{R}^{3\times 3}$ the identity matrix and the subscript notation f_* meaning evaluation at $\boldsymbol{v}_*$. In general, $\gamma > 0$ corresponds to hard potentials and $\gamma < 0$ to soft potentials. In particular, $\gamma = 1$ model hard spheres; $\gamma = 0$ are known as Maxwell molecules; and $\gamma = -3$ model Coulomb interactions between particles.

Since Fokker-Planck-Landau type equations are a limit of the Boltzmann equation, they enjoy the same conservation laws. In particular, for the set of collision invariants $\{\phi_k(\boldsymbol{v})\}_{k=0}^4 = \left\{1, v_1, v_2, v_3, |\boldsymbol{v}|^2\right\}$,

$$\int_{\mathbb{R}^3} Q(f, f)(\boldsymbol{v}) \phi_k(\boldsymbol{v}) \, \mathrm{d}\boldsymbol{v} = 0, \qquad \text{for } k = 0, 1, \ldots, 4. \tag{2}$$

This is important because it leads to the conservation of mass ρ, average velocity $\boldsymbol{V}$ and temperature T, where each of these quantities are found via

$$\rho = \int_{\mathbb{R}^3} f(t, \boldsymbol{v}) \, \mathrm{d}\boldsymbol{v}, \quad \boldsymbol{V} = \frac{1}{\rho} \int_{\mathbb{R}^3} f(t, \boldsymbol{v}) \boldsymbol{v} \, \mathrm{d}\boldsymbol{v} \quad \text{and} \quad T = \frac{1}{3\rho} \int_{\mathbb{R}^3} f(t, \boldsymbol{v}) |\boldsymbol{v} - \boldsymbol{V}|^2 \, \mathrm{d}\boldsymbol{v}.$$

These moments will always be conserved for the single-species homogeneous Landau equation (1) as well as for the corresponding space-inhomogenous version, if modeled with appropriate boundary conditions (e.g. reflective or periodic boundary conditions).

If the initial mass, average velocity and temperature are denoted by ρ_0, $\boldsymbol{V}_0$ and T_0, respectively, the equilibrium solution of the Landau equation is a Gaussian distribution with the same moments. This is referred to as the equilibrium Maxwellian, denoted by $\mathcal{M}_{eq}$, and is the specific Maxwellian distribution with moments equal to those of the initial condition, given by

$$\mathcal{M}_{eq}(\boldsymbol{v}) = \frac{\rho_0}{(2\pi T_0)^{\frac{3}{2}}} e^{-\frac{|\boldsymbol{v} - \boldsymbol{V}_0|^2}{2T_0}}.$$

Similarly, the H-theorem holds for Fokker-Planck-Landau type equations, which states that the entropy decays throughout time.

The entropy is defined as $$\mathcal{H}[f](t) = \int_{\mathbb{R}^3} f \log(f)\, \mathrm{d}\boldsymbol{v}$$

and so the H-theorem gives that $$\frac{\mathrm{d}}{\mathrm{d}t}\left(\mathcal{H}[f]\right) \leq 0.$$

At this point it is also useful to define the entropy relative to the equilibrium Maxwellian $\mathcal{M}_{eq}$ as

$$\mathcal{H}[f|\mathcal{M}_{eq}](t) = \int_{\mathbb{R}^3} f \log(f)\, \mathrm{d}\boldsymbol{v} - \int_{\mathbb{R}^3} \mathcal{M}_{eq} \log(\mathcal{M}_{eq})\, \mathrm{d}\boldsymbol{v} = \int_{\mathbb{R}^3} f \log\left(\frac{f}{\mathcal{M}_{eq}}\right) \mathrm{d}\boldsymbol{v}. \tag{3}$$

Initially $f(0, \boldsymbol{v}) = f_0(\boldsymbol{v})$ and it is assumed that $\mathrm{supp} f \Subset \Omega_{\boldsymbol{v}}$, since f should have sufficient decay in velocity-space [9] and $\Omega_{\boldsymbol{v}}$ is chosen depending on the initial data (see [13], section 2). In fact, $\boldsymbol{v} \in \mathbb{R}^3$ but values of f are negligible outside a sufficiently large ball. The initial data is then extended by zero outside the computational domain, which means it can be controlled by $e^{-c|\boldsymbol{v}|^2}$, for $c > 0$ depending on the moments of f_0. Under such conditions, it is expected that the computational solution will remain supported on $\Omega_{\boldsymbol{v}}$ up to a fixed small error that depends on the initial data (more details can be seen in the proof for the conservative spectral method applied to the Boltzmann equation in [13]).

Equation (1) is solved by the conservative spectral method with fourth order Runge-Kutta for time-stepping. Conservation is enforced by considering a constrained minimisation problem. Given a collection of discrete values of the collision operator, resulting from the spectral method, a new set of values must be found which are as close as possible to the original values in ℓ^2-norm but satisfy the discrete form of (2), where the integrals are replaced with quadrature sums. The solution to this problem is a matrix multiplication of the original values, where the matrix is identical for both the Boltzmann and Landau equations. The complete derivation can be found in [10] and [6] for the Boltzmann and Landau equations, respectively. As will be seen in the current work, the method also respects the correct decay rate of entropy. The spectral method will be described in the next section and is extended from the Landau equation with Coulomb interactions to Fokker-Planck-Landau type equations with Maxwell molecule and hard sphere interactions.

3 The Fourier Transform of the Collision Operator

As is shown in [6], when using a ball of radius $R > 0$ as the cut-off domain for computational purposes, the Fourier transform of the collision operator Q is

$$\hat{Q}(\hat{f}, \hat{f})(\boldsymbol{\xi}) = \int_{\Omega_{\boldsymbol{\xi}}} \hat{f}(\boldsymbol{\xi} - \boldsymbol{\omega})\, \hat{f}(\boldsymbol{\omega}) \Big(\boldsymbol{\omega}^T \hat{S}(\boldsymbol{\omega})\, \boldsymbol{\omega} - (\boldsymbol{\xi} - \boldsymbol{\omega})^T \hat{S}(\boldsymbol{\omega})\, (\boldsymbol{\xi} - \boldsymbol{\omega}) \Big)\, \mathrm{d}\boldsymbol{\omega}, \quad \text{for } \boldsymbol{\xi} \in \Omega_{\boldsymbol{\xi}} \subseteq \mathbb{R}^3, \tag{4}$$

where $$\hat{S}(\boldsymbol{\omega}) = (2\pi)^{-\frac{3}{2}} \int_{B_R(\mathbf{0})} S(\boldsymbol{u}) e^{-i\boldsymbol{\omega}\cdot\boldsymbol{u}} \mathrm{d}\boldsymbol{u}, \quad \text{for } S(\boldsymbol{u}) = |\boldsymbol{u}|^{\gamma+2} \left(\mathrm{I} - \frac{\boldsymbol{u}\boldsymbol{u}^T}{|\boldsymbol{u}|^2} \right), \quad \text{with } -3 \leq \gamma \leq 1.$$

This means that evaluating $\hat{Q}$ is performed by a fast Fourier transform (FFT) of the pdf f and then a weighted convolution with itself. The FFT requires $O(N^3 \log N)$ operations and multiplication by the weight and quadrature to calculate the convolution requires $O(N^3)$ operations. The weights can also be pre-computed and stored at the beginning of the code run, where the bulk of the calculation is in evaluation of $\hat{S}$. This has different forms depending on the value of γ but the results are found through the same general method.

First, the entries of $\hat{S}$ can be decomposed as $\hat{S}_{i,j}(\boldsymbol{\omega}) = \hat{S}^1_{i,j}(\boldsymbol{\omega}) - \hat{S}^2_{i,j}(\boldsymbol{\omega})$, for $i, j = 1, 2, 3$, with

$$\hat{S}^1_{i,j}(\boldsymbol{\omega}) = (2\pi)^{-\frac{3}{2}} \int_{B_R(\mathbf{0})} |\boldsymbol{u}|^{\gamma+2} \delta_{i,j} e^{-i\boldsymbol{\omega}\cdot\boldsymbol{u}}\, \mathrm{d}\boldsymbol{u} \quad \text{and} \quad \hat{S}^2_{i,j}(\boldsymbol{\omega}) = (2\pi)^{-\frac{3}{2}} \int_{B_R(\mathbf{0})} |\boldsymbol{u}|^{\gamma} u_i u_j e^{-i\boldsymbol{\omega}\cdot\boldsymbol{u}}\, \mathrm{d}\boldsymbol{u}. \tag{5}$$

Then, for a given $\boldsymbol{\omega} = (\omega_1, \omega_2, \omega_3)$, it should be noted that when $j = i$, there is only one value of $\hat{S}^1_{i,i}(\boldsymbol{\omega})$, for each $i = 1, 2, 3$, and that $\hat{S}^1_{i,j}(\boldsymbol{\omega}) = 0$ when $i \neq j$ (thanks to the Kronecker delta). Also note that

$$\hat{S}^2_{1,1}(\omega_1, \omega_2, \omega_3) = \hat{S}^2_{3,3}(\omega_2, \omega_3, \omega_1) \quad \text{and} \quad \hat{S}^2_{2,2}(\omega_1, \omega_2, \omega_3) = \hat{S}^2_{3,3}(\omega_1, \omega_3, \omega_2), \quad \text{for } i = j$$

and $$\hat{S}^2_{1,2}(\omega_1, \omega_2, \omega_3) = \hat{S}^2_{1,3}(\omega_1, \omega_3, \omega_2) \quad \text{and} \quad \hat{S}^2_{2,3}(\omega_1, \omega_2, \omega_3) = \hat{S}^2_{1,3}(\omega_2, \omega_1, \omega_3), \quad \text{for } i \neq j.$$

The sub-diagonal entries are then also known since $\hat{S}$ is a symmetric matrix (because S is symmetric). This means that only $\hat{S}^{\,1}_{1,1}$, $\hat{S}^{\,2}_{3,3}$ and $\hat{S}^{\,2}_{1,3}$ need to be calculated.

Now, in general, to calculate an integral of the form $(2\pi)^{-\frac{3}{2}} \int_{B_R(\mathbf{0})} G(\boldsymbol{u}) e^{-i\boldsymbol{\omega}\cdot\boldsymbol{u}} \, \mathrm{d}\boldsymbol{u}$ evaluated at $\boldsymbol{\omega}$ such that $|\boldsymbol{\omega}| \neq 0$, first a substitution is made in order to reduce the scalar product in the exponential to a single multiplication. To do this, note that the rotation matrix A given by

$$A = \begin{bmatrix} \frac{\omega_1\omega_3}{\sqrt{\omega_1^2+\omega_2^2}} & \frac{\omega_2\omega_3}{\sqrt{\omega_1^2+\omega_2^2}} & -\sqrt{\omega_1^2+\omega_2^2} \\ -\frac{\omega_2|\boldsymbol{\omega}|}{\sqrt{\omega_1^2+\omega_2^2}} & \frac{\omega_1|\boldsymbol{\omega}|}{\sqrt{\omega_1^2+\omega_2^2}} & 0 \\ \omega_1 & \omega_2 & \omega_3 \end{bmatrix}$$

has the property that $A\boldsymbol{\omega} = (0, 0, |\boldsymbol{\omega}|)$. Also, since A is a rotation matrix, it is orthogonal and so $A^{-1} = A^T$ and $\det A = 1$.

Then, changing variables via $\boldsymbol{u} = A^T\boldsymbol{w}$ and noting that $\boldsymbol{\omega}\cdot\boldsymbol{u} = \boldsymbol{\omega}^T A^T \boldsymbol{w} = (A\boldsymbol{\omega})^T\boldsymbol{w} = |\boldsymbol{\omega}| w_3$, gives

$$(2\pi)^{-\frac{3}{2}} \int_{B_R(\mathbf{0})} G(\boldsymbol{u}) e^{-i\boldsymbol{\omega}\cdot\boldsymbol{u}} \, \mathrm{d}\boldsymbol{u} = (2\pi)^{-\frac{3}{2}} \int_{B_R(\mathbf{0})} G\left(A^T\boldsymbol{w}\right) e^{-i|\boldsymbol{\omega}|w_3} \, \mathrm{d}\boldsymbol{w}.$$

Finally, by changing to spherical coordinates via

$$\boldsymbol{w} = r\boldsymbol{\sigma} = r(\sin(\theta)\cos(\phi), \sin(\theta)\sin(\phi), \cos(\theta)),$$

where $0 \leq r \leq R$, $-\pi \leq \phi \leq \pi$ and $0 \leq \theta \leq \pi$,

$$(2\pi)^{-\frac{3}{2}} \int_{B_R(\mathbf{0})} G(\boldsymbol{u}) e^{-i\boldsymbol{\omega}\cdot\boldsymbol{u}} \, \mathrm{d}\boldsymbol{u} = (2\pi)^{-\frac{3}{2}} \int_0^R \int_{-\pi}^{\pi} \int_0^{\pi} G\left(rA^T\boldsymbol{\sigma}\right) e^{-ir|\boldsymbol{\omega}|\cos(\theta)} r^2 \sin(\theta) \, \mathrm{d}\theta\mathrm{d}\phi\mathrm{d}r. \tag{6}$$

So, by using $G(\boldsymbol{u}) = |\boldsymbol{u}|^{\gamma+2}$ for $\hat{S}^{\,1}_{1,1}(\boldsymbol{\omega})$; $G(\boldsymbol{u}) = |\boldsymbol{u}|^{\gamma} u_3^2$ for $\hat{S}^{\,2}_{3,3}(\boldsymbol{\omega})$; and $G(\boldsymbol{u}) = |\boldsymbol{u}|^{\gamma} u_1 u_3$ for $\hat{S}^{\,2}_{1,3}(\boldsymbol{\omega})$, this means that the required weights from (5) are given by

$$\hat{S}^{\,1}_{1,1}(\boldsymbol{\omega}) = \begin{cases} \sqrt{\frac{2}{\pi}} \frac{1}{|\boldsymbol{\omega}|^2}\Big(1 - \cos(R|\boldsymbol{\omega}|)\Big), & \text{when } \gamma = -3, \\ \sqrt{\frac{2}{\pi}} \frac{1}{|\boldsymbol{\omega}|^5}\Big(-(R|\boldsymbol{\omega}|)^3\cos(R|\boldsymbol{\omega}|) + 3(R|\boldsymbol{\omega}|)^2\sin(R|\boldsymbol{\omega}|) + 6(R|\boldsymbol{\omega}|)\cos(R|\boldsymbol{\omega}|) - 6\sin(R|\boldsymbol{\omega}|)\Big), & \text{when } \gamma = 0, \\ \sqrt{\frac{2}{\pi}} \frac{1}{|\boldsymbol{\omega}|^6}\Big(-(R|\boldsymbol{\omega}|)^4\cos(R|\boldsymbol{\omega}|) + 4(R|\boldsymbol{\omega}|)^3\sin(R|\boldsymbol{\omega}|) + 12(R|\boldsymbol{\omega}|)^2\cos(R|\boldsymbol{\omega}|) \\ \qquad - 24(R|\boldsymbol{\omega}|)\sin(R|\boldsymbol{\omega}|) - 24\cos(R|\boldsymbol{\omega}|) + 24\Big), & \text{when } \gamma = 1, \end{cases}$$

$$\hat{S}^{\,2}_{3,3}(\boldsymbol{\omega}) = \begin{cases} \sqrt{\frac{2}{\pi}} \frac{1}{|\boldsymbol{\omega}|^4}\Big(\big(\omega_1^2+\omega_2^2\big)\frac{R|\boldsymbol{\omega}| - \sin(R|\boldsymbol{\omega}|)}{R|\boldsymbol{\omega}|} - \omega_3^2\frac{R|\boldsymbol{\omega}| + (R|\boldsymbol{\omega}|)\cos(R|\boldsymbol{\omega}|) - 2\sin(R|\boldsymbol{\omega}|)}{R|\boldsymbol{\omega}|}\Big), & \text{when } \gamma = -3, \\ \sqrt{\frac{2}{\pi}} \frac{1}{|\boldsymbol{\omega}|^7}\Big(\big(\omega_1^2+\omega_2^2\big)\Big(-(R|\boldsymbol{\omega}|)^2\sin(R|\boldsymbol{\omega}|) - 3(R|\boldsymbol{\omega}|)\cos(R|\boldsymbol{\omega}|) + 3\sin(R|\boldsymbol{\omega}|)\Big) \\ \qquad + \omega_3^2\Big(-(R|\boldsymbol{\omega}|)^3\cos(R|\boldsymbol{\omega}|) + 5(R|\boldsymbol{\omega}|)^2\sin(R|\boldsymbol{\omega}|) + 12(R|\boldsymbol{\omega}|)\cos(R|\boldsymbol{\omega}|) - 12\sin(R|\boldsymbol{\omega}|)\Big)\Big), & \text{when } \gamma = 0, \\ \sqrt{\frac{2}{\pi}} \frac{1}{|\boldsymbol{\omega}|^8}\Big(\big(\omega_1^2+\omega_2^2\big)\Big(-(R|\boldsymbol{\omega}|)^3\sin(R|\boldsymbol{\omega}|) - 4(R|\boldsymbol{\omega}|)^2\cos(R|\boldsymbol{\omega}|) + 8(R|\boldsymbol{\omega}|)\sin(R|\boldsymbol{\omega}|) \\ \qquad + 8\cos(R|\boldsymbol{\omega}|) - 8\Big) \\ \qquad + \omega_3^2\Big(-(R|\boldsymbol{\omega}|)^4\cos(R|\boldsymbol{\omega}|) + 6(R|\boldsymbol{\omega}|)^3\sin(R|\boldsymbol{\omega}|) + 20(R|\boldsymbol{\omega}|)^2\cos(R|\boldsymbol{\omega}|) \\ \qquad - 40(R|\boldsymbol{\omega}|)\sin(R|\boldsymbol{\omega}|) - 40\cos(R|\boldsymbol{\omega}|) + 40\Big)\Big), & \text{when } \gamma = 1 \end{cases}$$

and

$$\hat{S}^{\,2}_{1,3}(\boldsymbol{\omega}) = \begin{cases} -\sqrt{\dfrac{2}{\pi}}\dfrac{\omega_1\omega_3}{|\boldsymbol{\omega}|^4}\dfrac{2R|\boldsymbol{\omega}| + R|\boldsymbol{\omega}|\cos(R|\boldsymbol{\omega}|) - 3\sin(R|\boldsymbol{\omega}|)}{R|\boldsymbol{\omega}|}, & \text{when } \gamma = -3, \\ \sqrt{\dfrac{2}{\pi}}\dfrac{\omega_1\omega_3}{|\boldsymbol{\omega}|^7}\Big(-(R|\boldsymbol{\omega}|)^3\cos(R|\boldsymbol{\omega}|) + 6(R|\boldsymbol{\omega}|)^2\sin(R|\boldsymbol{\omega}|) + 15(R|\boldsymbol{\omega}|)\cos(R|\boldsymbol{\omega}|) - 15\sin(R|\boldsymbol{\omega}|)\Big), & \text{when } \gamma = 0, \\ \sqrt{\dfrac{2}{\pi}}\dfrac{\omega_1\omega_3}{|\boldsymbol{\omega}|^8}\Big(-(R|\boldsymbol{\omega}|)^4\cos(R|\boldsymbol{\omega}|) + 7(R|\boldsymbol{\omega}|)^3\sin(R|\boldsymbol{\omega}|) + 24(R|\boldsymbol{\omega}|)^2\cos(R|\boldsymbol{\omega}|) \\ \qquad - 48(R|\boldsymbol{\omega}|)\sin(R|\boldsymbol{\omega}|) - 48\cos(R|\boldsymbol{\omega}|) + 48\Big), & \text{when } \gamma = 1. \end{cases}$$

In addition, by substituting $\boldsymbol{\omega} = \mathbf{0}$ into the integrands found in $\hat{S}^{\,1}_{1,1}$, $\hat{S}^{\,2}_{3,3}$ and $\hat{S}^{\,2}_{1,3}$ from (5) and evaluating directly (noting that the exponential evaluated at $\boldsymbol{\omega} = \mathbf{0}$ is equal to one),

$$\hat{S}^{\,1}_{1,1}(\mathbf{0}) = \begin{cases} \sqrt{\dfrac{1}{2\pi}}R^2, & \text{when } \gamma = -3, \\ \dfrac{2}{5}\sqrt{\dfrac{1}{2\pi}}R^5, & \text{when } \gamma = 0, \\ \dfrac{1}{3}\sqrt{\dfrac{1}{2\pi}}R^6, & \text{when } \gamma = 1, \end{cases} \qquad \hat{S}^{\,2}_{3,3}(\mathbf{0}) = \begin{cases} \dfrac{1}{3\sqrt{2\pi}}R^2, & \text{when } \gamma = -3, \\ \dfrac{2}{15\sqrt{2\pi}}R^5, & \text{when } \gamma = 0, \\ \dfrac{1}{9\sqrt{2\pi}}R^6, & \text{when } \gamma = 1 \end{cases} \qquad \text{and} \quad \hat{S}^{\,2}_{1,3}(\mathbf{0}) = 0 \ \text{ (for all } \gamma).$$

4 Stability of the Space-homogeneous Spectral Method

In order to consider the stability of the spectral method, first note that the integral (4) to calculate $\hat{Q}$ is approximated using quadrature. The current code uses the composite trapezoidal rule but, in general, for M equally spaced quadrature nodes $\{\boldsymbol{\xi}_m\}_{m=1}^M$ in Fourier space, corresponding weights $\{w_m\}_{m=1}^M$ and Fourier space stepsize h_ξ,

$$\hat{Q}(\boldsymbol{\xi}_k) = h_\xi^3 \sum_{m=1}^{M} w_m \hat{f}(\boldsymbol{\xi}_k - \boldsymbol{\xi}_m)\,\hat{f}(\boldsymbol{\xi}_m)\Big(\boldsymbol{\xi}_m{}^T \hat{S}(\boldsymbol{\xi}_m)\,\boldsymbol{\xi}_m - (\boldsymbol{\xi}_k - \boldsymbol{\xi}_m)^T \hat{S}(\boldsymbol{\xi}_m)\,(\boldsymbol{\xi}_k - \boldsymbol{\xi}_m)\Big), \tag{7}$$

Now, according to Lebedev [16], the criterion for stability of a numerical method of the form

$$\frac{\mathrm{d}}{\mathrm{d}t}\Big(\hat{f}(\boldsymbol{\xi}_k)\Big) = F(\hat{f}(\boldsymbol{\xi}_k))$$

is that the time-stepsize Δt must satisfy

$$\Delta t \leq \frac{1}{\mathrm{Lip}(F)},$$

for the Lipschitz norm of F, $\mathrm{Lip}(F)$. If an upper bound can be found on $\mathrm{Lip}(F)$, this will in turn give a lower bound on $(\mathrm{Lip}(F))^{-1}$, which Δt must be below for the numerical method to remain stable. To find the upper bound, note that

$$\mathrm{Lip}(F) \leq |\mathcal{J}_{k,l}|, \quad \text{for the Jacobian } \mathcal{J}_{k,l} \text{ of } F(\hat{f}(\boldsymbol{\xi}_k)), \text{ given by } \mathcal{J}_{k,l} = \frac{\partial}{\partial \hat{f}(\boldsymbol{\xi}_l)}\Big(F(\hat{f}(\boldsymbol{\xi}_k))\Big).$$

Here, $F(\hat{f}(\boldsymbol{\xi}_k)) = \frac{1}{\varepsilon}\hat{Q}(\hat{f},\hat{f})(\boldsymbol{\xi}_k)$ and, to calculate the derivative of $\hat{Q}(\hat{f},\hat{f})(\boldsymbol{\xi}_k)$ with respect to $\hat{f}(\boldsymbol{\xi}_l)$, it should be noted that there are two chances for $\hat{f}(\boldsymbol{\xi}_l)$ to appear in the quadrature sum (7). These are when $m = l$ and in general (depending on the choice of quadrature nodes) at another index, say $m = n$, where $\boldsymbol{\xi}_k - \boldsymbol{\xi}_n = \boldsymbol{\xi}_l$. Assuming that there are indeed two indices which give rise to non-zero derivatives in the sum, and considering that $\boldsymbol{\xi}_k - \boldsymbol{\xi}_n = \boldsymbol{\xi}_l$ is equivalent to $\boldsymbol{\xi}_n = \boldsymbol{\xi}_k - \boldsymbol{\xi}_l$, the derivative is given by

$$\begin{aligned} \frac{\partial}{\partial \hat{f}(\boldsymbol{\xi}_l)}\Big(\hat{Q}(\hat{f},\hat{f})(\boldsymbol{\xi}_k)\Big) = {} & h_\xi^3 w_l \hat{f}(\boldsymbol{\xi}_k - \boldsymbol{\xi}_l)\Big(\boldsymbol{\xi}_l{}^T \hat{S}(\boldsymbol{\xi}_l)\,\boldsymbol{\xi}_l - (\boldsymbol{\xi}_k - \boldsymbol{\xi}_l)^T \hat{S}(\boldsymbol{\xi}_l)\,(\boldsymbol{\xi}_k - \boldsymbol{\xi}_l)\Big) \\ & + h_\xi^3 w_n \hat{f}(\boldsymbol{\xi}_n)\Big(\boldsymbol{\xi}_n{}^T \hat{S}(\boldsymbol{\xi}_n)\,\boldsymbol{\xi}_n - (\boldsymbol{\xi}_k - \boldsymbol{\xi}_n)^T \hat{S}(\boldsymbol{\xi}_n)\,(\boldsymbol{\xi}_k - \boldsymbol{\xi}_n)\Big) \\ = {} & h_\xi^3 w_l \hat{f}(\boldsymbol{\xi}_k - \boldsymbol{\xi}_l)\Big(\boldsymbol{\xi}_l{}^T \hat{S}(\boldsymbol{\xi}_l)\,\boldsymbol{\xi}_l - (\boldsymbol{\xi}_k - \boldsymbol{\xi}_l)^T \hat{S}(\boldsymbol{\xi}_l)\,(\boldsymbol{\xi}_k - \boldsymbol{\xi}_l)\Big) \\ & + h_\xi^3 w_n \hat{f}(\boldsymbol{\xi}_k - \boldsymbol{\xi}_l)\Big((\boldsymbol{\xi}_k - \boldsymbol{\xi}_l)^T \hat{S}(\boldsymbol{\xi}_k - \boldsymbol{\xi}_l)\,(\boldsymbol{\xi}_k - \boldsymbol{\xi}_l) - \boldsymbol{\xi}_l^T \hat{S}(\boldsymbol{\xi}_k - \boldsymbol{\xi}_l)\,\boldsymbol{\xi}_l\Big). \end{aligned} \tag{8}$$

Then, since $h_\xi = \frac{\pi}{L_v}$ and $|w_l| \leq 1$ for any l, by the triangle inequality,

$$\left|\frac{\partial}{\partial \hat{f}(\boldsymbol{\xi}_l)}\Big(\hat{Q}(\hat{f},\hat{f})\,(\boldsymbol{\xi}_k)\Big)\right| \leq \frac{\pi^3}{L_v^3}|\hat{f}\,(\boldsymbol{\xi}_k-\boldsymbol{\xi}_l)\,|\Big(|\boldsymbol{\xi}_l{}^T\hat{S}\;\;(\boldsymbol{\xi}_l)\,\boldsymbol{\xi}_l| + |(\boldsymbol{\xi}_k-\boldsymbol{\xi}_l)^T\hat{S}\;\;(\boldsymbol{\xi}_l)\,(\boldsymbol{\xi}_k-\boldsymbol{\xi}_l)\,| \\ + |(\boldsymbol{\xi}_k-\boldsymbol{\xi}_l)^T\hat{S}\;\;(\boldsymbol{\xi}_k-\boldsymbol{\xi}_l)\,(\boldsymbol{\xi}_k-\boldsymbol{\xi}_l)| + |\boldsymbol{\xi}_l^T\hat{S}\;\;(\boldsymbol{\xi}_k-\boldsymbol{\xi}_l)\,\boldsymbol{\xi}_l|\Big).$$

Note that if there had been no such $\boldsymbol{\xi}_n$ then the final two terms would be omitted here and the bound would only be smaller.

Also, by definition of the Fourier transform,

$$|\hat{f}\,(\boldsymbol{\xi}_k-\boldsymbol{\xi}_l)\,| \leq (2\pi)^{-\frac{3}{2}}\int_{B_R(\mathbf{0})}|f\,(\boldsymbol{u})\,||e^{-i(\boldsymbol{\xi}_k-\boldsymbol{\xi}_l)\cdot\boldsymbol{u}}|\mathrm{d}\boldsymbol{u} = (2\pi)^{-\frac{3}{2}}\|f\|_{L_1(B_R(\mathbf{0}))},$$

since $|e^{-i(\boldsymbol{\xi}_k-\boldsymbol{\xi}_l)\cdot\boldsymbol{u}}| = 1$, and so

$$\left|\frac{\partial}{\partial \hat{f}(\boldsymbol{\xi}_l)}\Big(\hat{Q}(\hat{f},\hat{f})\,(\boldsymbol{\xi}_k)\Big)\right| \leq \frac{\pi^{\frac{3}{2}}}{2\sqrt{2}L_v^3}\|f\|_{L_1(B_R(\mathbf{0}))}\Big(|\boldsymbol{\xi}_l{}^T\hat{S}\;\;(\boldsymbol{\xi}_l)\,\boldsymbol{\xi}_l| + |(\boldsymbol{\xi}_k-\boldsymbol{\xi}_l)^T\hat{S}\;\;(\boldsymbol{\xi}_l)\,(\boldsymbol{\xi}_k-\boldsymbol{\xi}_l)\,| \\ + |(\boldsymbol{\xi}_k-\boldsymbol{\xi}_l)^T\hat{S}\;\;(\boldsymbol{\xi}_k-\boldsymbol{\xi}_l)\,(\boldsymbol{\xi}_k-\boldsymbol{\xi}_l)| + |\boldsymbol{\xi}_l^T\hat{S}\;\;(\boldsymbol{\xi}_k-\boldsymbol{\xi}_l)\,\boldsymbol{\xi}_l|\Big). \quad (9)$$

Now, for the terms involving $\hat{S}$, note that for a general matrix $A \in \mathbb{R}^{3\times3}$ and vectors $\boldsymbol{y}, \boldsymbol{z} \in \mathbb{R}^3$,

$$\boldsymbol{y}^TA\boldsymbol{z} = \sum_{i,j=1}^{3}A_{i,j}y_iz_j \quad \text{and so} \quad |\boldsymbol{y}^TA\boldsymbol{z}| \leq (3)^2\max_{i,j=1,2,3}|A_{i,j}|(\max_{i=1,2,3}y_i)(\max_{i=1,2,3}z_i). \quad (10)$$

This means that a bound must be found on $|\hat{S}_{i,j}(\boldsymbol{\xi})|$, which is achieved by using the expressions in section 3 for $\hat{S}^{\,1}_{1,1}$, $\hat{S}^{\,2}_{3,3}$ and $\hat{S}^{\,2}_{1,3}$, for $\gamma = -3$, 0 and 1. It is shown in [15] that, for any $k = 1, 2, \ldots, M$,

$$|\hat{S}_{i,j}(\boldsymbol{\xi}_k)| \leq \begin{cases}\left(\sqrt{\dfrac{1}{2\pi}} + \dfrac{3}{\pi^3}\big(\pi+1\big)\sqrt{\dfrac{2}{\pi}}\right)L_v^2, & \text{when } \gamma=-3,\\ \sqrt{\dfrac{2}{\pi}}\dfrac{1}{\pi^5}\big(2\pi^3+9\pi^2+21\pi+21\big)L_v^5, & \text{when } \gamma=0,\\ \sqrt{\dfrac{2}{\pi}}\dfrac{1}{\pi^6}\big(2\pi^6+11\pi^3+36\pi^2+72\pi+144\big)L_v^6, & \text{when } \gamma=1\end{cases} \lesssim \begin{cases}L_v^2, & \text{when } \gamma=-3,\\ L_v^5, & \text{when } \gamma=0,\\ L_v^6, & \text{when } \gamma=1.\end{cases}$$

Then, by using the identity (10) and noting that $|(\boldsymbol{\xi}_k)_i| \leq L_\xi = \frac{\pi}{h_v}$, for any $k, l, n = 1, 2, \ldots, M$,

$$|\boldsymbol{\xi}_k^T\hat{S}\,(\boldsymbol{\xi}_l)\boldsymbol{\xi}_n| \lesssim 9\frac{\pi^2}{h_v^2}\times\begin{cases}L_v^2, & \text{when } \gamma=-3,\\ L_v^5, & \text{when } \gamma=0,\\ L_v^6, & \text{when } \gamma=1.\end{cases}$$

Now, since $\boldsymbol{\xi}_k - \boldsymbol{\xi}_l = \boldsymbol{\xi}_n$, each mixed $\boldsymbol{\xi}_k - \boldsymbol{\xi}_l$ and $\boldsymbol{\xi}_l$ term in inequality (9) has the same upper bound. This gives

$$\left|\frac{\partial}{\partial \hat{f}(\boldsymbol{\xi}_l)}\Big(\hat{Q}(\hat{f},\hat{f})\,(\boldsymbol{\xi}_k)\Big)\right| \lesssim 4\left(9\frac{\pi^{\frac{7}{2}}}{2\sqrt{2}h_v^2L_v^3}\|f\|_{L_1(B_R(\mathbf{0}))}\right)\times\begin{cases}L_v^2, & \text{when } \gamma=-3,\\ L_v^5, & \text{when } \gamma=0,\\ L_v^6, & \text{when } \gamma=1,\end{cases}$$

and so

$$|\mathcal{J}_{k,l}| \leq \frac{1}{\varepsilon}\left|\frac{\partial}{\partial \hat{f}(\boldsymbol{\xi}_l)}\Big(\hat{Q}(\hat{f},\hat{f})\,(\boldsymbol{\xi}_k)\Big)\right| \lesssim \frac{18\pi^{\frac{7}{2}}}{\sqrt{2}\varepsilon h_v^2}\|f\|_{L_1(B_R(\mathbf{0}))}\times\begin{cases}\dfrac{1}{L_v}, & \text{when } \gamma=-3,\\ L_v^2, & \text{when } \gamma=0,\\ L_v^3, & \text{when } \gamma=1,\end{cases}$$

which means

$$\frac{1}{|\mathcal{J}_{k,l}|} \gtrsim \begin{cases} \dfrac{\sqrt{2}\varepsilon L_v h_v^2}{18\pi^{\frac{7}{2}}\|f\|_{L_1(B_R(\mathbf{0}))}}, & \text{when } \gamma = -3, \\ \dfrac{\sqrt{2}\varepsilon h_v^2}{18\pi^{\frac{7}{2}} L_v^2\|f\|_{L_1(B_R(\mathbf{0}))}}, & \text{when } \gamma = 0, \\ \dfrac{\sqrt{2}\varepsilon h_v^2}{18\pi^{\frac{7}{2}} L_v^3\|f\|_{L_1(B_R(\mathbf{0}))}}, & \text{when } \gamma = 1. \end{cases}$$

Therefore, to ensure that $\Delta t \leq \frac{1}{|\mathcal{J}_{k,l}|}$, choose Δt such that

$$\Delta t \leq \begin{cases} \dfrac{\sqrt{2}\varepsilon L_v h_v^2}{18\pi^{\frac{7}{2}}\|f\|_{L_1(B_R(\mathbf{0}))}}, & \text{when } \gamma = -3, \\ \dfrac{\sqrt{2}\varepsilon h_v^2}{18\pi^{\frac{7}{2}} L_v^2\|f\|_{L_1(B_R(\mathbf{0}))}}, & \text{when } \gamma = 0, \\ \dfrac{\sqrt{2}\varepsilon h_v^2}{18\pi^{\frac{7}{2}} L_v^3\|f\|_{L_1(B_R(\mathbf{0}))}}, & \text{when } \gamma = 1 \end{cases} = \begin{cases} \dfrac{2\sqrt{2}\varepsilon L_v^3}{9\pi^{\frac{7}{2}} N^2\|f\|_{L_1(B_R(\mathbf{0}))}}, & \text{when } \gamma = -3, \\ \dfrac{2\sqrt{2}\varepsilon}{9\pi^{\frac{7}{2}} N^2\|f\|_{L_1(B_R(\mathbf{0}))}}, & \text{when } \gamma = 0, \\ \dfrac{2\sqrt{2}\varepsilon}{9\pi^{\frac{7}{2}} N^2 L_v\|f\|_{L_1(B_R(\mathbf{0}))}}, & \text{when } \gamma = 1. \end{cases}$$

5 Numerical Results and Entropy Decay

5.1 The Coulomb Case ($\gamma = -3$)

The purpose of this example is to numerically verify the rate of convergence to equilibrium, proven analytically by Strain and Guo [14]. They show in their paper that, for $-3 \leq \gamma < 0$, there is no spectral gap for Fokker-Planck-Landau type equations. Instead, when the initial condition is bounded by $e^{-c|\boldsymbol{v}|^2}$, for some $c > 0$, the rate of convergence to a Maxwellian close to equilibrium is given by

$$e^{-kt^p}, \quad \text{with } p = -\frac{2}{\gamma} \text{ and some } k > 0.$$

For Coulomb interactions, with $\gamma = -3$, this gives the law of two thirds. To verify this numerically, the natural log of the relative entropy is plotted on a log-log scale against time. In particular, as the solution approaches equilibrium, it should be that

$$\log\Big(\Big|\log(\big|\mathcal{H}[f|\mathcal{M}_{eq}]\big|)\Big|\Big) \sim \frac{2}{3}\log(t).$$

In order to demonstrate this, an initial condition far from equilibrium is chosen. In particular, the initial condition used is a sum of four Maxwellians with shifted centers, namely

$$f_0(\boldsymbol{v}) = \frac{1}{4}\sum_{l=0}^{3} \mathcal{M}_v\left(\boldsymbol{v} + \left((-1)^{\lfloor \frac{l}{2} \rfloor}, (-1)^l, (-1)^l\right)\right), \tag{11}$$

for the Maxwellian $\mathcal{M}_v(\boldsymbol{v}) = (2\pi T)^{-\frac{3}{2}} e^{-\frac{|\boldsymbol{v}|^2}{2T}}$. The marginal of this initial condition is plotted in Fig. 1(a), where it can be seen that this has the form of four humps. The temperature used is $T = 0.4$; the Knudsen number is $\varepsilon = 20$; the velocity domain has $L_v = 5.25$; $N = 16$ Fourier modes are chosen; and the time-stepsize used is $\Delta t = 0.01$ (below the upper bound of approximately 0.0646 calculated for stability with these parameters for $\gamma = -3$ in section 4).

The simulations are carried out with C++ code run on the Texas Advanced Computing Center's Stampede2 supercomputer [17], utilizing all sixty eight cores on the Intel Xeon Phi 7250 1.4GHz Knights Landing processor using OpenMP [18]. Any procedure that requires a loop over the grid-cells in velocity space distributes the cells amongst the OpenMP threads then recombines the individual values calculated at the end of the loop. Table 1 records the times taken for 100 time-steps of the current simulation with various numbers of threads (averaged over three runs), which shows that the performance increase is almost linear in the number of threads.

TABLE 1: Average times after three runs of 100 time-steps with various number of OpenMP threads on an Intel Xeon Phi 7250 1.4GHz Knights Landing processor in TACC's Stampede2 supercomputer

No. of OpenMP threads	1	2	4	8	16	32	68
Average time for 100 time-steps (seconds)	18,259	9,656	4,741	2,371	1,188	598	288

Marginals of the approximation to the Landau equation starting at the initial condition (11) are plotted at mean-free times $t = 2.8$, 20 and 100 in Fig. 1(b)-(d). This shows that the four humps merge together into one, before eventually taking shape as the equilibrium Maxwellian $\mathcal{M}_{eq}$ (see Fig. 1(d)) which, in this case with $T = 0.4$ in (11), has equilibrium temperature $T_{eq} = 1.4$ and is given by

$$\mathcal{M}_{eq}(\boldsymbol{v}) = \frac{1}{(2.8\pi)^{\frac{3}{2}}} e^{-\frac{|\boldsymbol{v}|^2}{2.8}}. \tag{12}$$

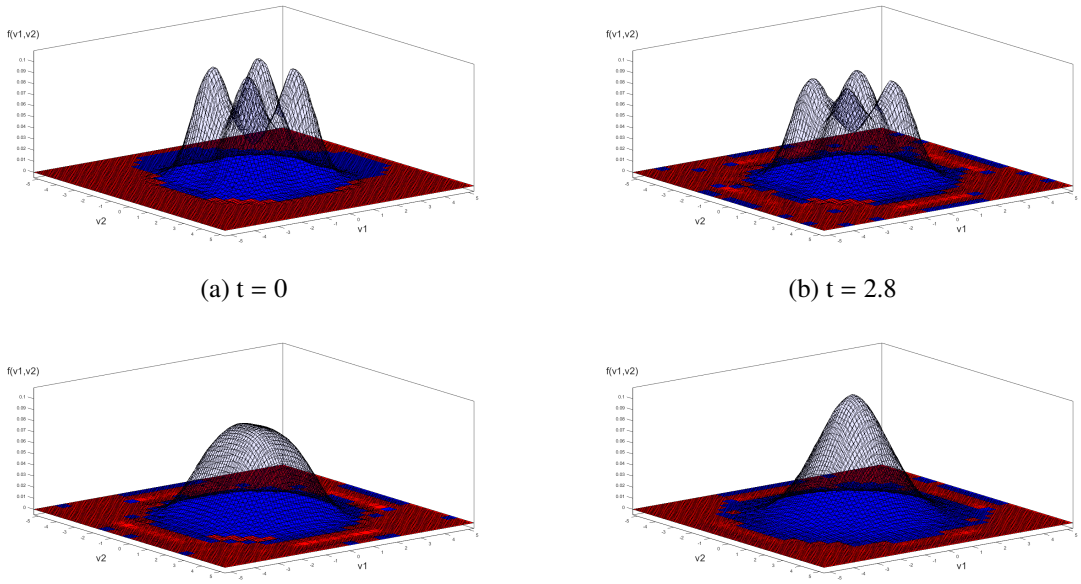

(a) t = 0 (b) t = 2.8

(c) t = 20 (d) t = 100

FIGURE 1: Marginals of f in the variables v_1 and v_2 at various times during the simulation of the Landau equation starting with the initial condition (11), with $T = 0.4$, $\varepsilon = 20$, $L_v = 5.25$, $N = 16$ and $\Delta t = 0.01$, showing cells in the domain where the solution is negative (in red, near the boundary) and positive (in blue, in the interior).

In Fig. 2, the relative entropy has been plotted. At this point, it should be noted that the numerical scheme does not preserve positivity. There is potential for negativity to occur when conservation is enforced. The good news, however, is that the negative parts of the solution only appear as a result of tiny oscillations near the tail. The negative regions are shown underneath the marginal plots in Fig. 1, on the (v_1, v_2)-axes, as red cells which are indeed next to the boundary near the tails. In these regions, the solution is negligible anyway and so the effects of the negative values are not noticed. Obviously, calculating the natural log in expression (3) for the relative entropy requires only positive values. Since the negative values are so tiny though (and the parts of the solution so close to zero give negligible influence on any bulk quantities anyway), these are just discarded when calculating the entropy. More precisely, the entropy is calculated through a quadrature method and any point for which f has a negative value is considered a zero contribution to the overall sum.

When natural logarithms have been taken, the curve does indeed become a straight line when close to equilibrium. It can be seen that, when $t = 2.8$ (corresponding to Fig. 1(b)), the curve is not yet straight but that is because the solution is still far from a Maxwellian. At around $t = 20$ (corresponding to Fig. 1(c)), however, the four humps have disappeared and the solution is becoming close to that of a Maxwellian. This is part of the entropy plot which is a straight line, with a slope of approximately 0.634, which is fairly close to two thirds, as hoped.

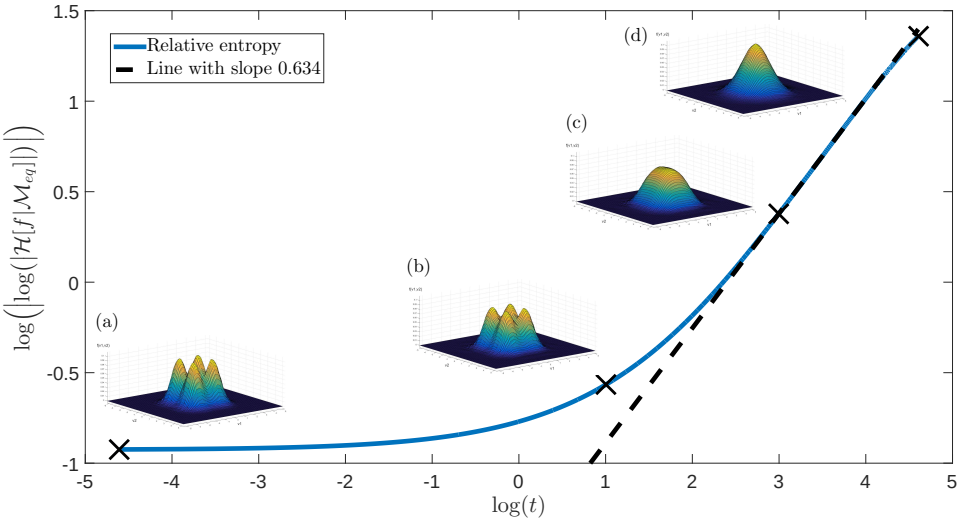

FIGURE 2: Plot of $\log\left(\left|\log\left(\left|\mathcal{H}[f|\mathcal{M}_{eq}]\right|\right)\right|\right)$ against $\log(t)$ for the numerical approximation f to the Landau equation, given initial condition (11), with $T = 0.4$, $\varepsilon = 20$, $L_v = 5.25$, $N = 16$ and $\Delta t = 0.01$, which has equilibrium solution $\mathcal{M}_{eq}$ given by (12). A straight line has been added to show that the slope near equilibrium is close to two thirds, exhibiting the lack of spectral gap, but a degenerate spectrum corresponding to a stretch-time exponential decay given by e^{-kt^p}, with $p = \frac{2}{3}$ and some $k > 0$. The labels correspond to the marginal plots in Fig. 1.

The importance of the conservation routine should also be noted here. The numerical scheme was run with the same parameters as above but without enforcing conservation and the deviations of mass and kinetic energy from their initial values during this simulation are plotted in Fig. 3(a). When the conservation routine is applied, to produce the results of Fig. 1-2, the mass and energy were held constant to machine accuracy. Here, however, there is a significant deviation of $O(10^{-2})$ showing that there is no hope of convergence to the Maxwellian with the same moments as the initial data. Nevertheless, a plot of the relative entropy has also been included in Fig. 3(b). Another problem here is that the entropy in the simulation without conserved moments drops below that of the theoretical equilibrium entropy, resulting in the spike around $\log(t) \approx 4.35$. There is still an exponential decay of relative entropy, however, as demonstrated by the straight line with a slope of approximately 0.6119. As expected, this is not as accurate as the slope of 0.634 when conservation is enforced.

5.2 The Hard Sphere Case ($\gamma = 1$)

Unlike when $\gamma < 0$, there is a spectral gap when $\gamma = 1$. This means the rate of convergence to a Maxwellian close to equilibrium is in fact exponential, of the form e^{-kt}, for some $k > 0$. Similar to the previous example, when close to equilibrium, the relative entropy should behave like $\log\left(\left|\log\left(\left|\mathcal{H}[f|\mathcal{M}_{eq}]\right|\right)\right|\right) \sim \log(t)$.

Trying to simulate hard spheres introduced a fair amount of difficulty, which shed light on an issue that should be considered for modeling hard potentials with the current spectral method. In particular, when choosing an initial condition for which the bulk of the mass is supported in too small a region near the center of the domain, the tails of the solution start to ripple after a small number of time-steps, causing an instability which leads to a blow-up. It is believed that this problem stems from the fact that collisions are much more significant for hard potentials than soft ones, with more weight being given to larger relative velocities. The relative velocity becomes larger when closer to the tails in velocity-space.

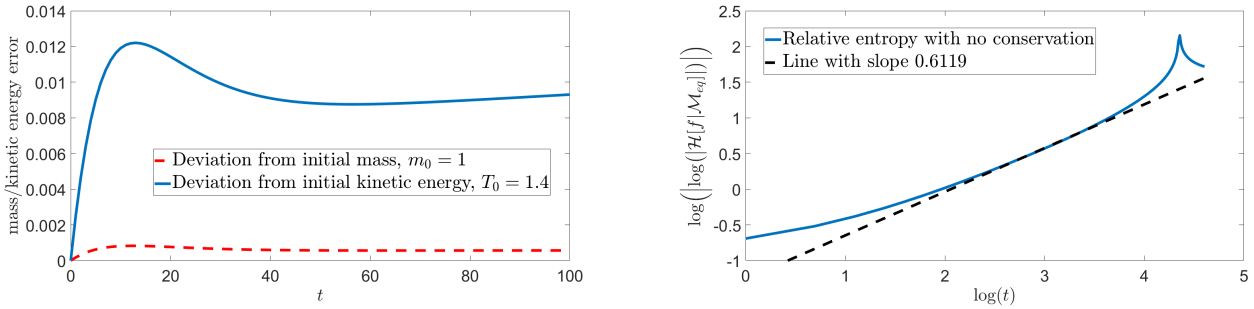

(a) (b)

FIGURE 3: Results from a simulation without the conservation routine, starting with the initial condition (11), with $T = 0.4$, $\varepsilon = 20$, $L_v = 5.25$, $N = 16$ and $\Delta t = 0.01$. (a) Plots of the error in the mass and kinetic energy from the initial values $m_0 = 1$ and $T_0 = 1.4$, respectively. (b) Plot of $\log\Big(\Big|\log\big(\big|\mathcal{H}[f|\mathcal{M}_{eq}]\big|\big)\Big|\Big)$ against $\log(t)$ for the numerical approximation f, which has equilibrium solution $\mathcal{M}_{eq}$ given by (12). A straight line has been added to show that the slope near equilibrium is approximately 0.6119, which is less than the slope 0.634 calculated when conservation is enforced.

At first, it may seem like a more compactly supported initial solution may help. The problem, however, is that collisions are computed in Fourier space. The Fourier transform will take a solution with small support in the original space and spread it out in the Fourier domain (consider, for example, that a Gaussian with large peak and small variance has a Gaussian with small peak and large variance as its Fourier transform). This means that the Fourier transform of such an initial condition actually has tails with rather large magnitude near the boundaries. When multiplied by the hard sphere weights calculated in section 3, this causes a problem computationally. This issue did not exist for $\gamma = -3$ as the weights near the tails for Coulomb interactions are smaller in magnitude. As a result, any part of the solution that turns negative is emphasized, which introduces the ripples as the conservation routine attempts to compensate.

For the hard sphere simulation, a very similar initial condition was chosen, namely

$$f_0(\boldsymbol{v}) = \frac{1}{4}\sum_{l=0}^{3} \mathcal{M}_v\left(\boldsymbol{v} + 0.02\left((-1)^{\lfloor \frac{l}{2} \rfloor}, (-1)^l, (-1)^l\right)\right), \tag{13}$$

for the Maxwellian $\mathcal{M}_v(\boldsymbol{v}) = (2\pi T)^{-\frac{3}{2}} e^{-\frac{|\boldsymbol{v}|^2}{2T}}$, with a smaller temperature of $T = 0.00025$ than for the Coulomb interactions example. Again, the Knudsen number is $\varepsilon = 20$ and $N = 16$ Fourier modes are used, but a much smaller velocity domain is chosen here, with boundary $L_v = 0.1$. This allows the time-stepsize to be increased slightly, as the stability results from section 4 show that a larger value of L_v requires a smaller time-stepsize for stability. Still, a smaller time-stepsize than for the Coulomb interaction example is used, namely $\Delta t = 0.0001$ (below the upper bound of approximately 0.00447 calculated for stability with these parameters for $\gamma = 1$ in section 4). The marginal plots are not included for this example, as they look almost identical to those in Fig. 1 from the Coulomb interactions example.

A plot of the relative entropy for hard spheres is shown in Fig. 4. When logarithms are taken, the curve is close to a straight line with slope 0.71742 which is less than the slope of one that is expected for a spectral gap. Nevertheless, this is still larger than the slope of two thirds for Coulomb interactions and the slope of one is merely an upper bound, so this result is still relatively satisfactory.

One final point to mention here is that the hard sphere simulations do not need to run for quite as long. This can be seen by noticing that the time axis is shorter in Fig. 4 than in Fig. 2. The shorter time is a consequence of the fact that the decay toward equilibrium with hard potentials is exponential, thanks to the existence of the spectral gap, which is faster than the stretch-time exponential decay for soft potentials. This is due to the collision frequency increasing as the relative velocity grows in the hard sphere model, giving a faster decay rate to equilibrium. Indeed, this simulation is under different conditions to the true Landau equation modeled in section 5.1, but the larger temperature in that initial condition should not influence the time taken to reach equilibrium. This is a result of the fact that, for Coulomb interaction with $\gamma = -3$, collisions are much weaker as the relative velocity increases and so larger temperatures will have very little influence.

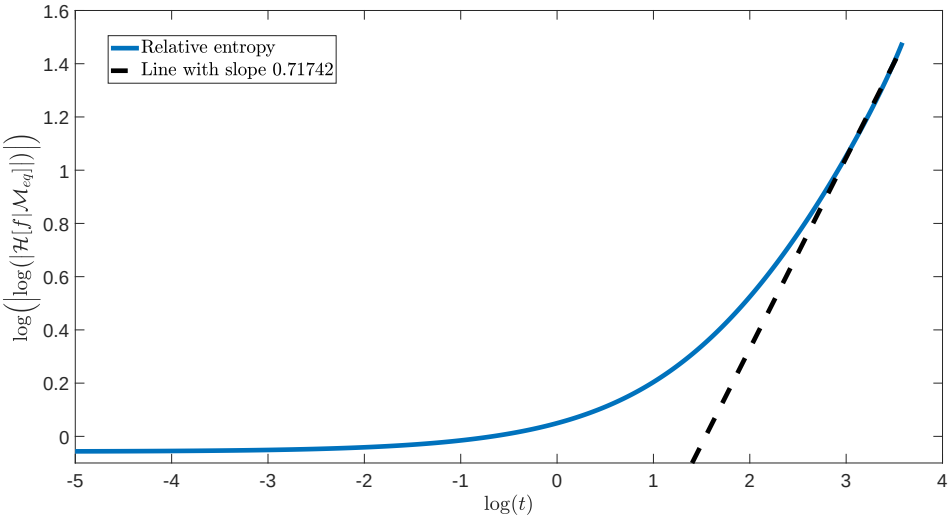

FIGURE 4: Plot of $\log\left(\left|\log(\left|\mathcal{H}[f|\mathcal{M}_{eq}]\right|)\right|\right)$ against $\log(t)$ for the numerical approximation f to the Fokker-Planck-Landau type equation with $\gamma = 1$ and weights calculated by the exact formulae in section 3, given initial condition (13), with $T = 0.00025$, $\varepsilon = 20$, $L_v = 0.1$, $N = 16$ and $\Delta t = 0.0001$, which has equilibrium solution given by a Maxwellian with temperature $T_{eq} = 0.0009750$. A straight line has been added to show that the slope near equilibrium is now approximately 0.71742, slightly below the value of one expected for the existence of a spectral gap.

6 Conclusion

In this work, the conservative spectral method for solving space-homogeneous Fokker-Planck-Landau type equations was expanded upon by extending the calculations to hard spheres and Maxwell molecules. Conditions for stability were then derived for each of the three cases. Finally, examples of the numerical method for Coulomb interactions and hard spheres were given to show the power of the scheme. In particular, the relative entropy during a simulation was shown to decay close to the correct rate for Coulomb interactions, in accordance with the rate of two thirds predicted by Strain and Guo, which shows that this code is an excellent model for the Landau equation. When the model is applied to the Fokker-Planck-Landau type equation with hard spheres interactions, the existence of the spectral gap is less evident but it is believed that this result can be improved upon by altering the parameters. The importance of the conservation routine was also demonstrated by showing that the decay rate without it is less accurate. Indeed, the method does not preserve positivity but the regions in which the solution falls below zero are always near the tails and the solution is negligible there anyway. Clearly this is true as dropping those values in calculation of the entropy did not detract too much from the result.

The code is easily expandable to the space-inhomogeneous case by use of a discontinuous Galerkin method and time-splitting. The simulations behave just as expected, also with negligible effects resulting from negative points in the distribution, and similar decay rates to equilibrium are observed. These results will be featured in an upcoming manuscript [15]. In addition, work is currently underway to implement the present method in a multi-species setting, based on the calculations by Gamba et al. [19] to develop an asymptotic preserving explicit-implicit numerical scheme for species with disparate masses.

7 ACKNOWLEDGMENTS

The authors would like to thank Chenglong Zhang for help in understanding the code used to implement the conservative spectral method and being available to give advice on any developments. Both authors have been partially funded by grants from the NSF. The Institute for Computational Engineering Sciences has also been incredibly supportive.

REFERENCES

[1] L. Landau, Phys. Zs. Sov. Union **10**, 154–164 (1936).

[2] C. Villani, Archive for Rational Mechanics and Analysis **143**, 273–307 (1998).

[3] L. Desvillettes and C. Villani, Communications in Partial Differential Equations **25**, 179–298 (2000).

[4] A. Bobylev and I. Potapenko, J. Comput. Phys. **246**, 123–144 (2013).

[5] J. Haack and I. Gamba, Conservative deterministic spectral Boltzmann solver near the grazing collisions limit, 28th rarefied gas dynamics conference, AIP Conference Proceedings (2012).

[6] C. Zhang and I. Gamba, J. Comput. Physics **340**, 470–497 (2017).

[7] A. Bobylev and S. Rjasanow, Eur. J. Mech. B Fluids **18**, 869–887 (1999).

[8] L. Pareschi, G. Russo, and G. Toscani, J. Comput. Physics **165**, 216–236 (2000).

[9] I. Gamba, V. Panferov, and C. Villani, Arch. Rational Mech. Anal. **194**, 253–282 (2009).

[10] I. Gamba and S. Tharkabhushaman, J. Comput. Physics **228**, 2012–2036 (2009).

[11] F. Filbet and L. Pareschi, J. Comput. Physics **179**, 1–26 (2002).

[12] N. Crouseilles and F. Filbet, J. Comput. Physics **201**, 546–572 (2004).

[13] R. Alonso, I. Gamba, and S. Tharkabhushaman, SIAM Num. Anal. **56**, 3534–3579 (2018).

[14] R. Strain and Y. Guo, Arch. Rational Mech. Anal. **187**, 287–339 (2008).

[15] C. Pennie and I. Gamba, work in progress (2019).

[16] V. Lebedev, "How to solve stiff systems of differential equations by explicit methods; numerical methods and applications *(1994)*," in *Numerical methods and applications* (CRC Revivals) 1st ed.

[17] The University of Texas at Austin, Texas Advanced Computing Center, http://www.tacc.utexas.edu (TACC).

[18] OpenMP Architecture Review Board, OpenMP Application Program Interface Version 3.0, http://www.openmp.org/mp-documents/spec30.pdf (May 2008).

[19] I. Gamba, S. Jin, and L. Liu, submitted for publication (2018).